journal

J. Am. Ceram. Soc., 94 [3] 633–646 (2011)
DOI: 10.1111/j.1551-2916.2011.04384.x
© 2011 The American Ceramic Society

Measuring and Interpreting the Structure of Grain-Boundary Networks

Gregory S. Rohrer†

Department of Materials Science and Engineering, Carnegie Mellon University, Pittsburgh, Pennsylvania 15213-3890

Recently developed techniques to measure the structure of interfacial networks in three dimensions have the potential to revolutionize our ability to control the microstructures of polycrystals and interface-dominated materials properties. This paper reviews recent findings from two- and three-dimensional orientation mapping studies. The observations confirm a strong inverse correlation between the relative energies of grain boundaries and the frequency with which they occur in microstructures. The observations also show that during microstructure evolution, relatively higher energy grain boundaries are more likely to be shrinking while lower energy interfaces are more likely to be growing. These processes can lead to a steady-state distribution of grain boundaries that is influenced as much by the relative grain-boundary energies as by the exact processing conditions. Recent findings and emerging opportunities for grain-boundary characterization are reviewed in the final section of the paper.

I. Introduction

THE paper is an account of the Robert B. Sosman lecture that was presented by the author on October 28, 2009, at the 111th Annual Meeting of the American Ceramic Society in Pittsburgh, PA. This paper presents an overview of progress during the past ten years toward understanding the mesoscale structure of grain boundaries and the networks they form within polycrystals. The paper will concentrate on findings from my students and colleagues in the Materials Research Science and Engineering Center at Carnegie Mellon University, which was founded in 1996 to study the mesoscale structure of polycrystalline materials. Three previous reviews of this topic have summarized the early work and the present paper is intended to focus on more recent progress and opportunities for the future.[1–3]

From the time of Kingery's[4]; seminal Sosman lecture in 1974 through today, grain boundaries have been a subject of interest to ceramic scientists.[5,6] The reason for this interest is clear: the vast majority of the solid materials used in engineered systems are polycrystalline. In other words, they are comprised of many single crystals joined together by a three-dimensional internal network of grain boundaries. In many cases, the performance and integrity of a material are determined by the mesoscale structure of the grain-boundary network. In the present context, mesoscale refers to the structural scale between the atomic scale and the macroscale and the principal characteristics of the mesoscale structure are the relative areas of different types of grain boundaries and the way that they are connected. When a local property such as corrosion resistance, electrical conductivity, or slip transmission depends on the grain-boundary type, then the associated macroscopic property of the polycrystal will be influenced or even dominated by the mesoscale structure.

The relative areas of different types of grain boundaries are described by the grain-boundary character distribution (GBCD). The grain-boundary type is specified by five parameters.[7] As parameters for this distribution, we select a misorientation type by specifying an axis-angle combination, and then plot the relative areas of grain-boundary planes on a stereographic projection (see Panel A). Anisotropic grain-boundary properties, such as the energy or mobility, can be parameterized in exactly the same way. The details of the methods used to calculate these distributions are provided in a previous review.[1]

In the past, it was typical to characterize the GBCD using fewer than five parameters. For example, it is possible to classify boundaries by the disorientation angle (a single parameter description, illustrated in Panel A(a)) or the axis and angle of disorientation (a three parameter description, illustrated in Panel A(b)). The reason to use a classification scheme with a reduced number of parameters is that the five-parameter space of grain-boundary types is large; if the space is discretized in 10° intervals, then there are roughly 6×10^3 different grain boundaries for a material with cubic symmetry.[1] The number of distinct boundaries increases rapidly for finer discretizations and crystals with reduced symmetry. So, until recently, the number of distinct grain-boundary types was large compared with the number of observations it was possible to make. However, this is no longer the case. The development of high-speed electron backscatter diffraction (EBSD) mapping of orientations has made it possible to characterize and classify 10^4 to 10^5 boundaries.[9,10]

It is reasonable to ask why one should go make the effort to measure all five crystallographic grain-boundary parameters. The reason is that both individual grain-boundary properties and macroscopic materials properties vary with all five parameters. For example, Matsunaga *et al.*[11] have observed substantial variations in the creep rate of Σ7 grain boundaries in alumina (boundaries with a 38.2° misorientation about [0001]) that depend on the grain boundary plane. Data on the relative energies

D. J. Green—contributing editor

Manuscript No. 28812. Received October 22, 2010; approved December 9, 2010.
The work was supported by the MRSEC program of the National Science Foundation under Award Number DMR-0520425.
†Author to whom correspondence should be addressed. e-mail: gr20@andrew.cmu.edu

Feature

Panel A. Description of multidimensional representations of grain boundary character distributions.

Three different representation of the distribution of relative areas of different types of grain boundaries, using the same data. This example is for a hexagonal material, WC. (a) This is a single-parameter disorientation distribution. Each boundary is classified by its minimum misorientation angle, without consideration of the misorientation axis. Compared with the random distribution, there is an enhancement of grain boundaries with 30° and 90° disorientation. (b) When one considers the axis and angle of the misorientation, there are three independent parameters for each boundary, two for axis direction and one for the rotation angle. Therefore, each position in a three-dimensional space corresponds to a different grain boundary. In each layer of the axis angle space, all possible axis are represented; the rotation angle varies along the vertical direction. Note that the peak for 30° in (a) is concentrated at [0001], indicating that these are mostly 30° rotations about [0001], and the peak at 90° is concentrated at [10-10], indicating that this is the dominant misorientation axis. For any particular axis angle combination, there is a distribution of grain-boundary planes, as shown for the examples in (c) and (d). Note that when the misorientation axis, the misorientation angle, and the grain-boundary planes are specified, there are five independent parameters. The grain-boundary plane distributions (c) and (d) are the relative areas of different grain-boundary planes at for the misorientation of 90° about [10-10] (c) 30° about [0001]. The plots are stereographic projections. The maxima show that the 90° [10-10] misorientation boundaries are concentrated on [10-10] planes, indicating that they are also pure twist boundaries. The local maxima at the prismatic misorientation correspond to asymmetric tilt boundaries.[8]

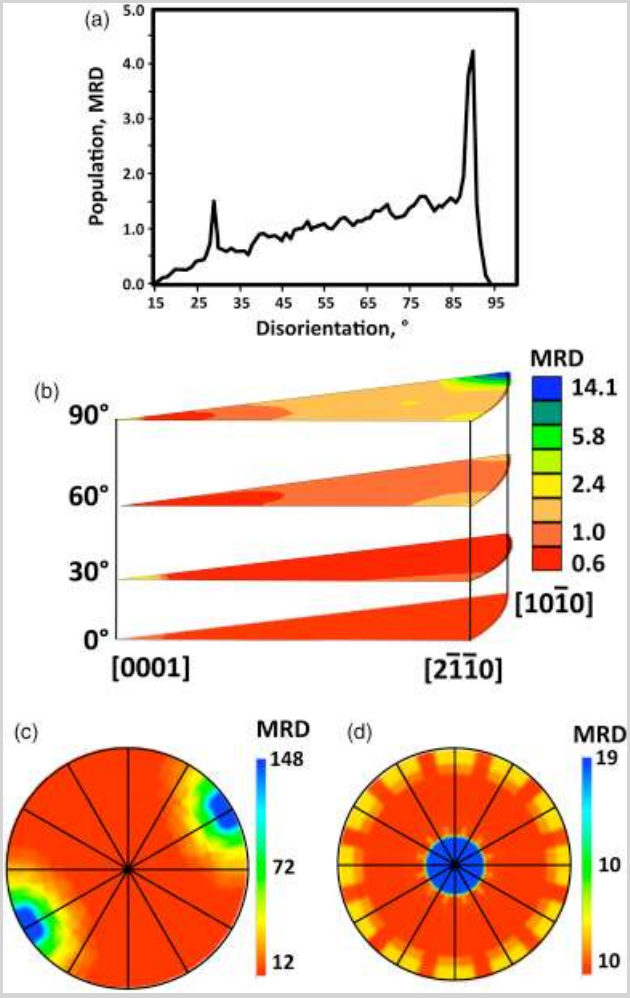

of [110] symmetric tilt grain boundaries in MgO and NiO also show a large effect of the grain-boundary plane.[12,13] In this tilt series, there are two Σ3 grain boundaries: one at a tilt angle of 70.5° and another at 109.5°. The 70.5° tilt boundary is a coherent twin bounded by (111) planes. These boundaries have the identical lattice misorientation, but different grain-boundary planes. For the case of MgO, the energy of the 109.5° Σ3 boundary is 40% higher than the 70.5° boundary. For the case of NiO, the energy of the 109.5° Σ3 boundary is 300% higher than the 70.5° boundary. The grain-boundary plane orientation parameters can also affect macroscopic properties. Finite element calculations have shown that residual thermal stresses in anisotropic materials vary both with the distribution of misorientations and grain-boundary plane orientations.[14]

II. The Emergence of New Techniques to Measure GB Distributions and Energies

Automated EBSD, which makes it possible to accumulate a map of orientations on a surface, has had a transformative effect on the study of grain boundaries in polycrystals (see Panel B).[10] It is

Panel B. Description of orientation mapping by electron backscatter diffraction mapping.

EBSD is used to map orientations in polycrystalline samples.[9,10] The experiment is conducted in an SEM with the sample titled at a large angle with respect to the beam (a). A digital camera captures a diffraction pattern (b) that is characteristics of the volume of material that interacted with the beam. The pattern is automatically indexed to specify the local orientation of the interaction volume. The beam is then moved a fixed distance and the process is repeated. After recording local orientations on a grid of points, an "inverse pole figure map" (c) can be plotted. The map shows the local orientations in the crystal reference frame with reference to the sample normal direction. The relationship between color and orientation are defined by the standard triangle below. This is a tetragonal sample.

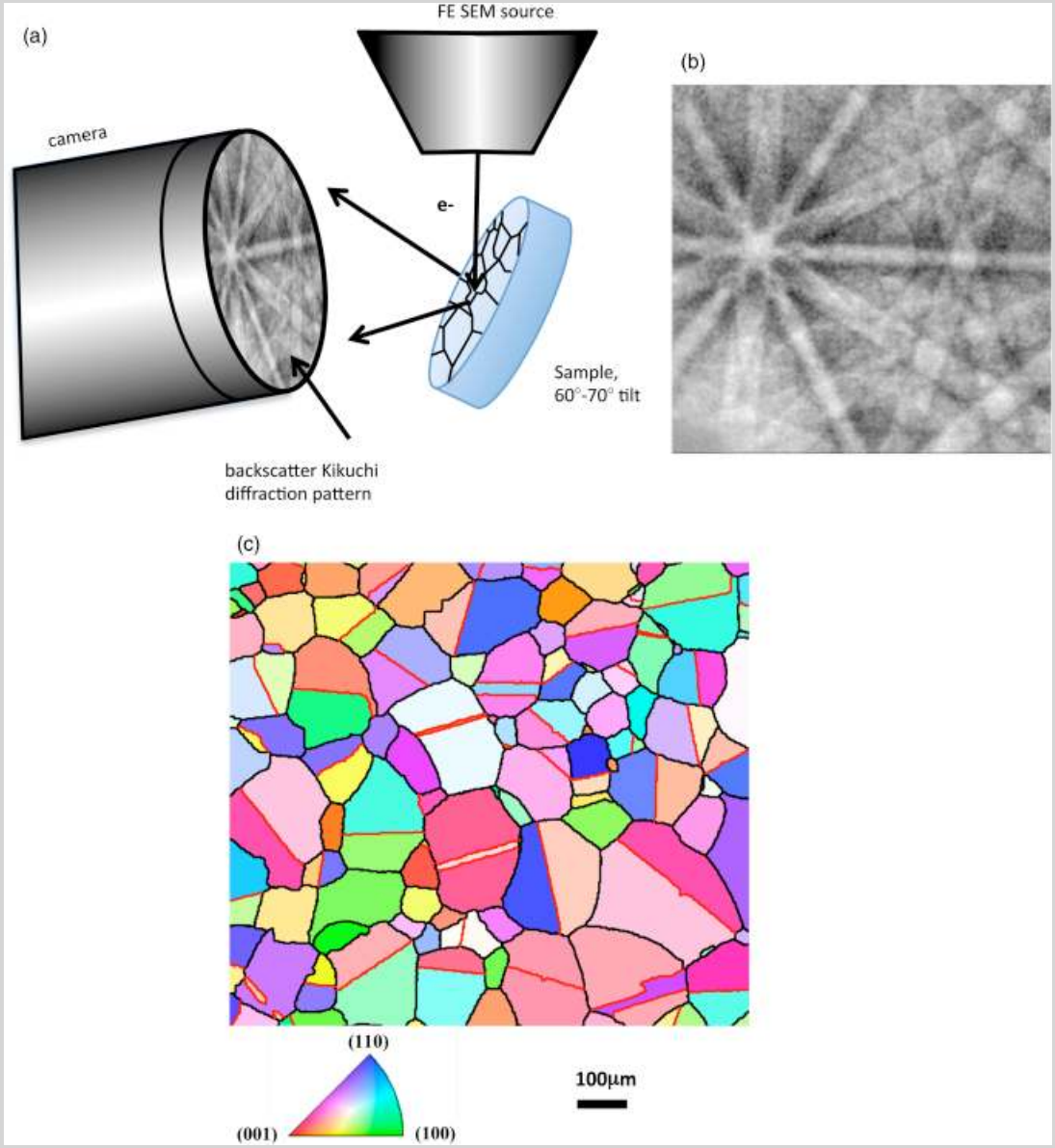

currently possible measure several hundred orientations per second, enabling the determination of the shapes and orientations of thousands of grains in a reasonable amount of time. In orientation maps such as that shown in Panel B, four of the five grain-boundary parameters can be specified: the lattice misorientation and the in plane component of the grain-boundary plane orientation. The most common way to make an absolute determination of the final component of the boundary plane orientation is remove a small amount of material (small compared with the grain size) and repeat the measurement; a process referred to as serial sectioning. Manual serial sectioning coupled with EBSD to determine grain-boundary plane crystallography is technically demanding and time consuming. As a result, there are relatively few examples in the literature.[15–21] It is also possible to calculate the GBCD through the stereological analysis of two-dimensional orientation maps.[22] Because this is much easier than serial sectioning, it has been more widely adopted.[8,23–44] The main limitation of stereology is that, in its current form, it can not be applied to materials with significant orientation texture.

The experimental barriers imposed by serial sectioning have been significantly reduced by dual beam microscopes that contain both an electron beam for EBSD mapping, and a focused ion beam (FIB) for material removal.[45–52] The sequence of ori-

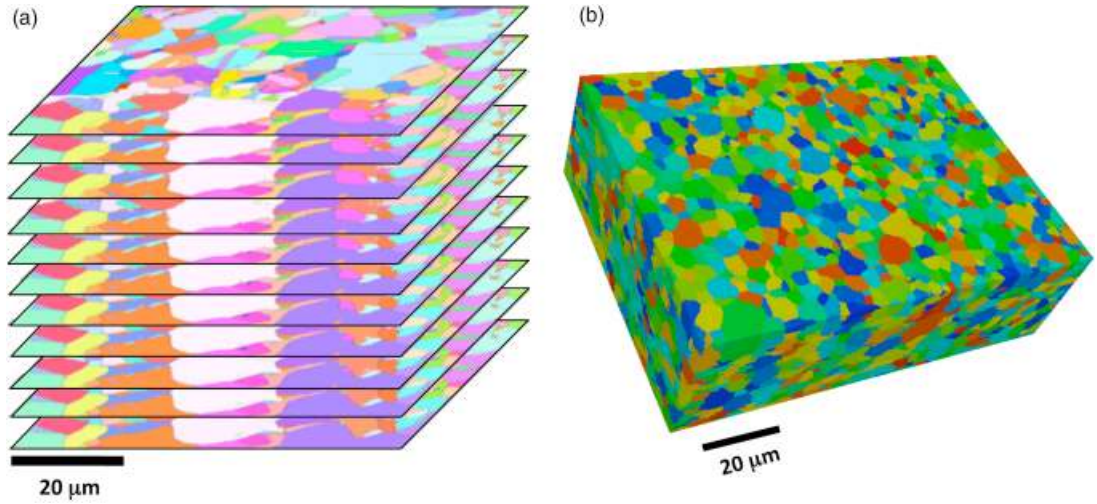

Fig. 1. (a) Stack of eleven EBSD maps from parallel layers separated by 200 nm in a Ni polycrystal.[51] The maps are shown in oblique projection to emphasize the three-dimensional structure of the data. (b) A three-dimensional orientation map based on 43 parallel EBSD maps from a yttria polycrystal.[50]

entation mapping and removing thin layers can be fully automated so that data can be acquired without user intervention. This has enabled the collection of large three-dimensional images of materials from which statistical information can be derived. An example is illustrated in Fig. 1. The three-dimensional images can also be used as the input to simulations of materials response.[53–55]

Grain-boundary energies can be evaluated from the geometries of surface triple junctions (grain-boundary thermal grooves) or internal grain-boundary triple junctions.[56–58] The geometries of these junctions carry an imprint of the interfacial energies (see Panel C). A key assumption in the process of extracting energies from interfacial geometries is that the triple lines where three interfaces meet are in local thermodynamic equilibrium and that this equilibrium is described by the Herring[57] equation. Surface observations, made using atomic force microscopy, sometimes ignore torques and do not account for grain-boundary inclination.[59–62] However, by measuring a large number of grooves, it is possible to compare the mean value and width of the distributions. The three-dimensional data can also be used to extract relative grain-boundary energies without any assumptions.[50–52,63] In this case, the equilibrium condition is

Panel C. Description of the condition for interfacial equilibrium at triple lines.

Interfacial junctions carry an "imprint" of the interfacial energies; the relationship between energy and geometry is described by the Herring[57] equation, shown below. This is vector balance of forces tangential and normal to the interface. The tangential forces, shown in blue, amount to a three-way tug-of-war at the triple junction. If one interface has a higher energy, it will pull the triple line along its tangent, annihilating the high-energy interface and replacing it by the lower energy interfaces. The normal forces, shown in red and often referred to as torques, result from anisotropy. If the differential of the energy with respect to rotation angle β is large, there is a normal force to rotate the boundary in the direction that lowers the energy. For the junction to be in equilibrium, the six forces must balance. This equation can be applied to triple junctions or thermal grooves at surfaces.[56]

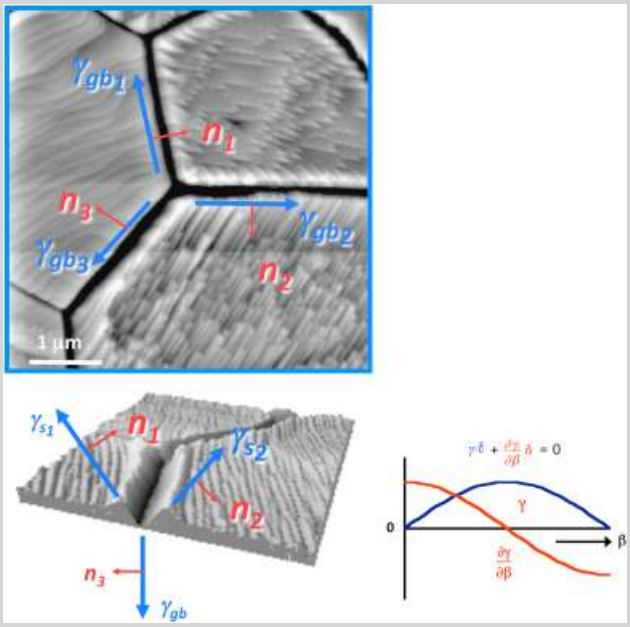

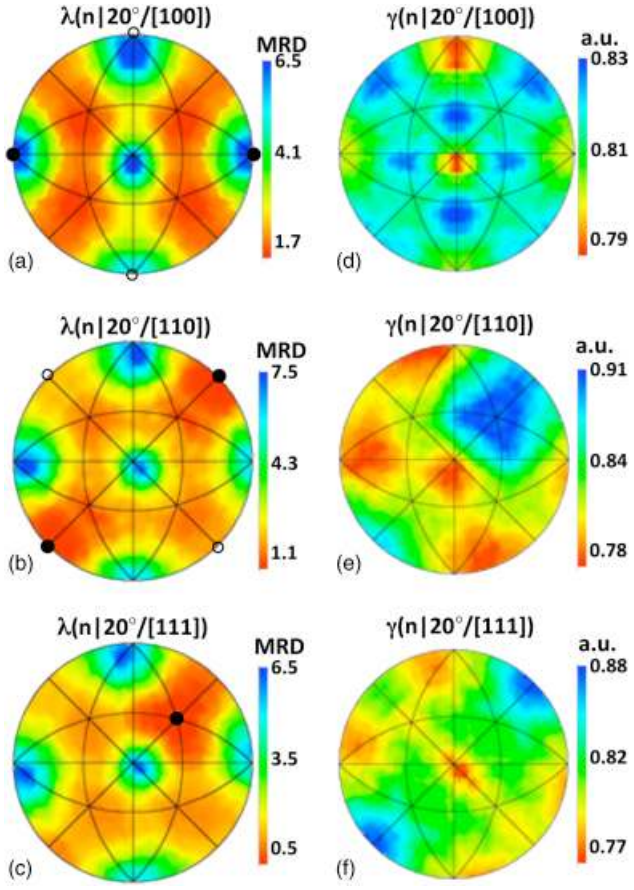

Fig. 2. Grain-boundary populations (a–c) and relative grain-boundary energies (d–f) for 20° misorientations about the [100] (a, d), [110] (b, e), and [111] (c, f) axes for polycrystalline Ca-doped MgO.[18,63] The distributions are plotted on stereographic projections, with [001] normal to the plane of projection and [100] along the horizontal direction in the plane of projection. All of the stereograms in this paper use the same reference frame. In (a–c), the orientations of the pure twist grain boundaries are marked with a filled black circle. In (a and b), the tilt boundaries are along the line between the unfilled circles.

expressed in terms of capillarity vectors as proposed by Cahn and colleagues[64,65] and Morawiec's[58]; procedure is then used to determine a set of capillarity vectors that best satisfies the equilibrium condition at all triple junctions. In this process, the possible grain boundaries are classified into a finite number of discrete types such that the number of observed triple junctions exceeds the number of unknown grain-boundary types.

III. Recent Findings about Grain Boundaries

One of the first significant findings in our studies of the mesoscale structure of polycrytsals was that grain-boundary plane distributions are anisotropic.[1,18,23] In other words, when the misorientation of the grain boundary is fixed, some grain-boundary plane orientations are more common than others. This is illustrated by the data in Fig. 2, which shows that in MgO, grain-boundary planes prefer (100) orientations.[18,63] The preference for certain low-index grain boundary planes occurs in a wide range of metallic and ceramic materials. The anisotropy of the grain-boundary plane distribution arises early in the genesis of the microstructure and, at least on average, has been observed to be invariant with grain size.[66] The results in Fig. 3 show the distribution of grain-boundary planes in $SrTiO_3$ at grain sizes between 3 and 23 μm; within the expected experimental uncertainty, they are indistinguishable.[66]

The grain-boundary plane distributions are found to exhibit an inverse correlation with grain-boundary energy distributions. In other words, low-energy boundaries make up a larger fraction of the distribution than higher energy boundaries. For the specific grain-boundary plane distributions shown in Figs. 2(a)–(c), a comparison with the relative energy distributions (Figs. 2(d)–(f)) shows that local maxima in the populations usually correlate with minima in the energy. The histograms in Fig. 4 illustrate that when all of the data are considered, the inverse correlation persists.[51,52,63] It is noteworthy that the low-energy boundaries have larger average areas and occur more frequently than expected.[19] The distributions are also sensitive to segregating impurities, as is illustrated by the comparison of the grain-boundary plane distributions for MgO with a variety of dopants (see Fig. 5).[35] This is presumably because of the effect that the impurities have on the grain-boundary energy anisotropy.

The measurement of grain-boundary distributions over all possible types of grain boundaries has provided a new perspective on which types of grain boundaries are common and have low energies. When one considers all of the data together, it can be concluded that the well known coincident site lattice model[67–69] is not a good predictor of grain-boundary energies.[19,24,70] One reason for this is that the CSL model only specifies the lattice misorientation of the boundary and, as noted above, there can be significant variation in energy and population as a function of grain-boundary plane. For example, Fig. 6 shows the grain-boundary plane distributions for the four highest coincidence grain boundaries in $SrTiO_3$.[19] Note that the populations of these grain boundaries do not exhibit maxima larger than what are found at low coincidence boundaries. Furthermore, even if we compare the orientations that have high planar coincidence (the symmetric tilt and twist boundaries marked in the figure), there is still no indication that these boundaries are significant with respect to energy or population. There are occasions when boundaries of high coincidence do have high populations and low energies. An example is the coherent twin in fcc metals, which is also a Σ3 boundary. However, comparisons across all high coincidence boundaries for a variety of materials provide no support for the idea that high coincidence alone leads to reduced energy.[19,24,70]

On the other hand, the one thing that does correlate with the presence of low-energy, high population boundaries is the presence of low index, low-energy surfaces.[19,23,63] As illustrated in

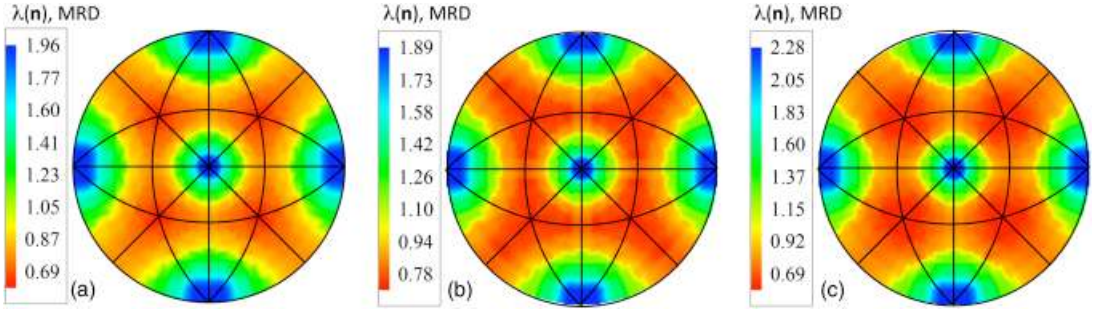

Fig. 3. Grain-boundary plane distributions for $SrTiO_3$ at different grain sizes. In this cases, the grain-boundary distributions are plotted without consideration of the misorientation.[66] Average grain sizes are 2.82 μm (a), 12.1 μm (b), and 23.2 μm (c).

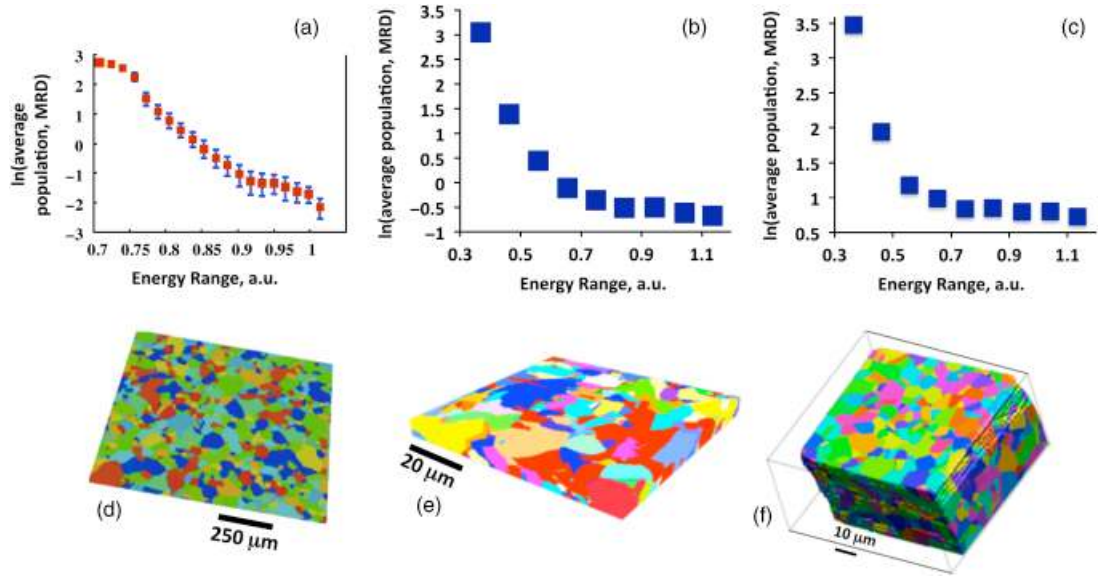

Fig. 4. Histograms of grain-boundary population versus grain-boundary energy (a–c) derived from three-dimensional microstrucutural data (c–e). In each case, the populations of all grain boundaries with energies within a fixed range were averaged to determine the population at each energy. The data is from MgO[63] (a, c), high purity Ni[51] (b, d), and a Ni-base super alloy (c, e).[115]

Fig. 7, the most commonly occurring grain-boundary plane orientations are correlated with low index, low-energy surface planes.[23,71–73] In fact, rather than seeking high symmetry configurations, the boundaries tend to favor configurations in which at least one side of the interface can be terminated by a low index plane. The energy cost for making a grain boundary can be thought of as the energy to create the two surfaces on either side of the interface, minus the binding energy that is recovered by bringing the two surfaces together.[74–77] The observation that the total grain-boundary energy is correlated to the surface energies suggests that surface energy anisotropies make more of a contribution to the total anisotropy than the binding energy. As a final note, it should be mentioned that while the statements above apply to grain boundaries with misorientation angles $>10°$, the same measurements indicate the energies of low misorientation angle grain boundaries are best described by the well established dislocation model of Read and Shockley.[63,78]

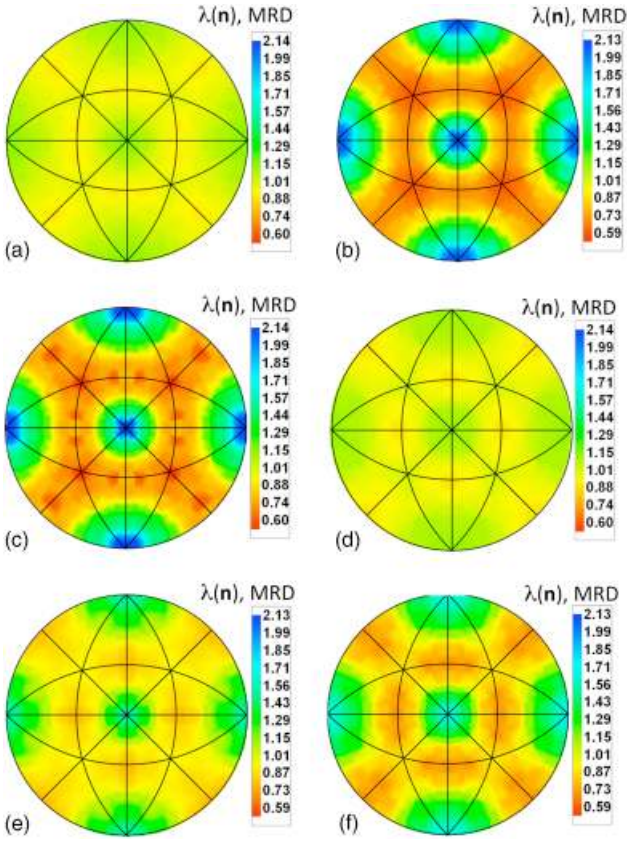

Fig. 5. Grain-boundary plane distributions, independent of misorientation, in the crystal reference frame for MgO polycrystals with different compositions. (a) undoped MgO, (b) 0.3% Ca-doped MgO, (c) 0.1% Ca-doped MgO, (d) Sr-doped MgO, (e) Ba-doped MgO, and (f) Y-doped MgO.[35]

IV. Model for the Development of Anisotropic Distributions

The observations described above do not by themselves provide a mechanism for how anisotropic distributions develop. If we imagine ceramics made by compacting and sintering equiaxed

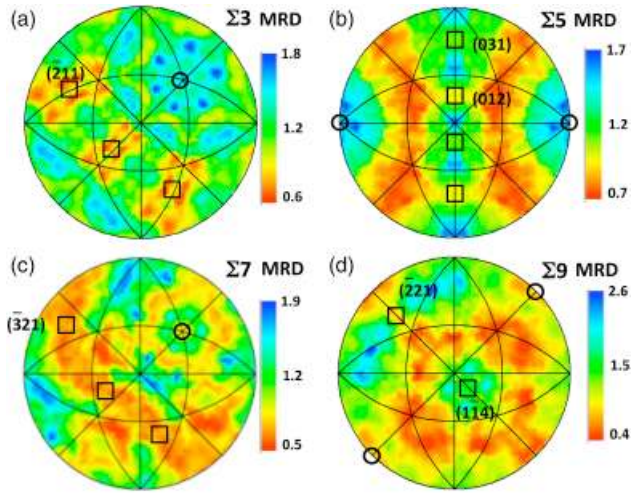

Fig. 6. Observed grain-boundary plane orientation distributions for (a) Σ3 (60°/[111]), (b) Σ5 (37°/[100]), (c) Σ7 (38°/[111]), and (d) Σ9 (39°/[110]) misorientations in $SrTiO_3$. In each plot, the squares mark the position of the symmetric tilt boundaries and the circles the positions of the pure twist boundaries. (a) twist: (111), tilt: $\bar{2}11$), ($\bar{1}\bar{1}2$), and ($1\bar{2}1$) (b) twist: (100) and ($\bar{1}00$) tilt: (031), (012), ($0\bar{1}3$), and ($0\bar{2}1$) (c) twist: (111), tilt: ($\bar{3}21$), ($\bar{2}\bar{1}3$) and ($1\bar{3}2$) (d) twist (110) and ($\bar{1}\bar{1}0$), tilt ($\bar{2}21$) and ($1\bar{1}4$).[19]

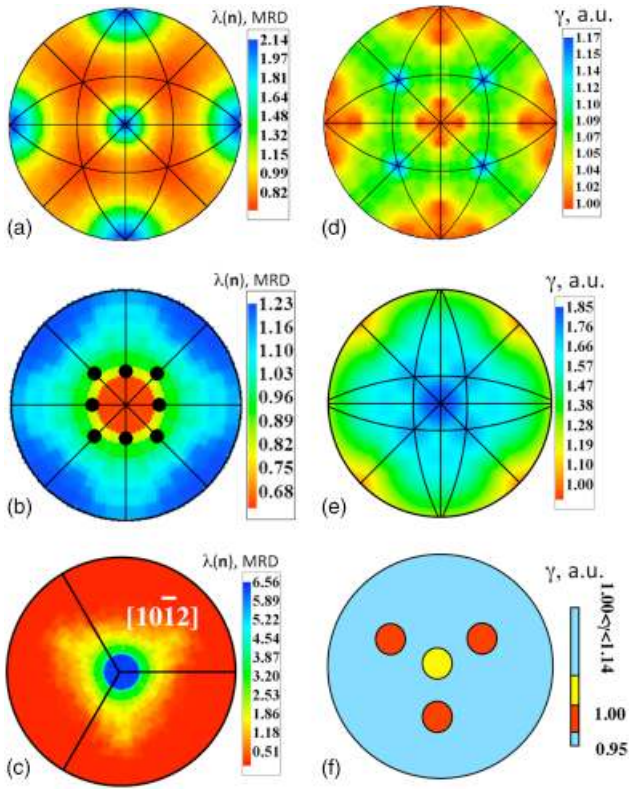

Fig. 7. Grain-boundary plane orientation distributions, independent of misorientation, for (a) MgO,[18] (b) TiO_2,[23] and (c) Al_2O_3 are compared to measured surface energies for (d) MgO,[60,62] (e) TiO_2,[72] and (f) Al_2O_3.[71] In each case, the lowest surface energy orientations correspond to larger than expected populations.

particles, it seems reasonable to assume that at some initial stage of microstructure development, the distribution of grain-boundary types is isotropic. Therefore, in the absence of specialized processing routes that have been developed to disrupt isotropy,[79,80] how do the anisotropic distributions arise from initially isotropic distributions? Computer simulations of grain growth confirm that anisotropic distributions can arise from initially isotropic distributions, that the distributions are inversely related to the energy anisotropy, and that mobility anisotropy is ineffective in creating anisotropic distributions.[81–84] On the other hand, the simulations provide limited insight into the mechanism by which anisotropic distributions develop.

While some grains are increasing in size during grain growth, the process of grain elimination occurs simultaneously. We hypothesized that higher energy boundaries, which on average have smaller areas, are preferentially eliminated from the distribution during grain growth. To test this idea, we correlated the energies of specific grain boundaries, estimated from measurements of their thermal grooves, with whether or not the boundary was increasing or decreasing in size.[85]

The AFM image in Fig. 8(a) shows a plane section of a yttrium aluminum garnet polycrystal. The surface has been thermally etched to groove the grain boundaries. The curvature of an individual boundary indicates its direction of motion. Note that in a section plane, each boundary is connected to four other grain boundaries. In some cases, the curvatures of the four attached boundaries indicate that as they migrate toward their center of curvature, the central boundary is increasing in size and in other cases the curvatures indicate that the central boundary is decreasing in size. The third and more common case is that there is a mixture of curvatures and it is not possible to determine how the area of the boundary is changing. Dividing the measured grain-boundary dihedral angles into three groups based upon this criterion, and using them to estimate the relative grain boundary to surface energy ratio,[56] a clear trend emerges

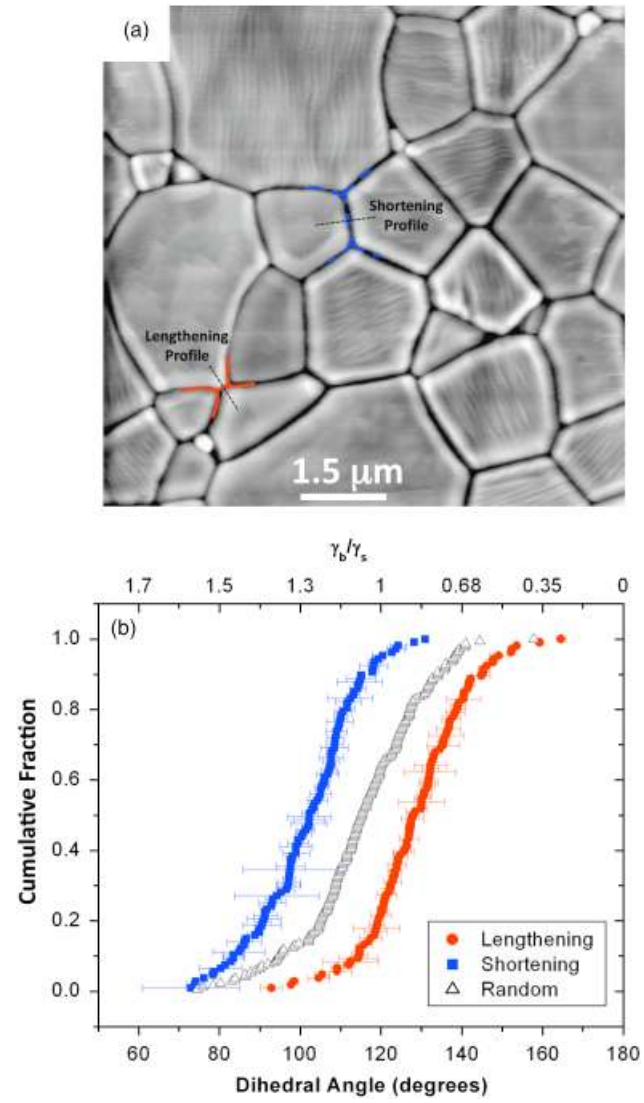

Fig. 8. (a) Contact AFM image of a thermally grooved yttrium aluminum garnet surface, with examples of boundaries that are growing and shrinking labeled. (b) Distribution of dihedral angles for the thermal grooves of growing, shrinking, and random boundaries on the surface of magnesia-doped alumina. The error bars represent the standard deviation from three measurements on each boundary.[85]

(see Fig. 8(b)). This result demonstrates that, as hypothesized, those boundaries decreasing in size have, on average, relative energies that are larger than those that are increasing in size. It was also observed that grain boundaries with higher average energies have smaller average areas.[85]

A simple model for the evolution of the GBCD can be developed based upon this principle.[86] First, It should be recognized that there are only three processes that alter the number fractions of grain boundaries. The first is that two grains can grow together to create a new boundary. The second is that two grains can pull apart, annihilating a boundary and leaving a triple line between them. These two processes, which are identical except for the directions of the two grains, are illustrated in Fig. 9. The third process is the collapse of a four-sided grain. The first process is the only one that creates new boundaries and the second process is the principal grain boundary annihilation mechanism. Therefore, we construct an equation for the rate at which boundaries are created and annihilated based upon estimates of the rates of the first two processes.

We begin by dividing the types of boundaries into N categories and assume that there are n_i boundaries of the ith type. The probability that a single event (e) changes n_i is the probability that a boundary of this type is created, minus the probability

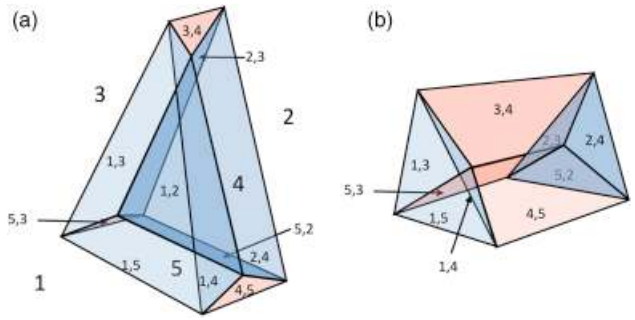

Fig. 9. (b) Representation of a triangular grain face between grains labeled 1 and 2. Each grain face is labeled by the adjoining grains. Grains 3, 4, and 5 surround the face and, with grains 1 and 2, complete the triple lines that bound the triangle. (b) If the face collapses, it is replaced by the triple line formed where grains 3, 4, and 5 meet. Transitioning from (a) to (b) corresponds to grain face annihilation and transitioning from (b) to (a) corresponds to grain face creation.

that a boundary of this type is eliminated. Under the assumption of random grain orientations (no texture), the probability that a particular type of grain boundary is created is the same as the probability of finding this boundary in a random distribution (ρ_i). Because higher energy boundaries have been observed to be more likely to be eliminated and have smaller areas, it was assumed that the probability of elimination was directly proportional to number of boundaries of that type and inversely proportional to the area ($\alpha = 1/\text{area}$), where the area is a function of the energy. With these considerations, the probability that a single event changes n_i can be expressed in the following way:

$$\frac{\Delta n_i}{\Delta e} = \left(\rho_i - \frac{\alpha_i n_i}{\sum_{i=1}^{N} \alpha_i n_i} \right) \quad (1)$$

Beginning with the assumption that the initial distribution is isotropic ($n_i = 1$) and that the energy is anisotropic, it is found that the grain-boundary distribution evolves to a steady state, anisotropic grain-boundary population distribution that is inversely related to the energy (see Fig. 10). These results are consistent with (but not identical to) the main observations of the experimental studies and suggest that the energy biased elimination of high-energy grain boundaries is a plausible mechanism for the development of anisotropic GBCDs. A more sophisticated model with the same underlying principles has recently been developed based on mesoscale simulations and the new model makes it possible to invert an observed population distribution to determine an energy distribution.[87,88]

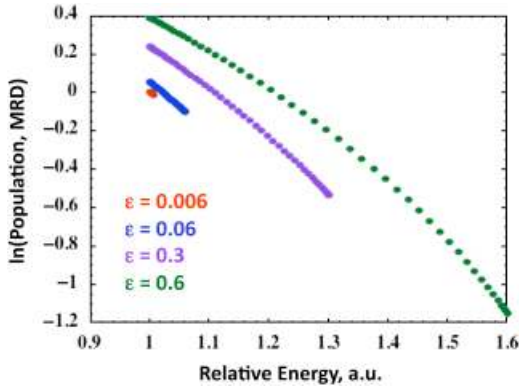

Fig. 10. A histogram of the steady-state grain-boundary population as a function of grain-boundary energy predicted by the critical event model, for four different magnitudes of the energy anisotropy, ε.[85]

V. Emerging Opportunities for Grain-Boundary Characterization

Although considerable progress has been made in the last decade in measuring and understanding grain-boundary networks in polycrystals, there remains much we do not know and there are several emerging techniques and areas of inquiry that provide us with new opportunities. For example, computational homology tools make it possible to study grain-boundary connectivity, high-energy X-ray diffraction techniques make it possible to nondestructively map orientations, and computational techniques make it possible to calculate realistic grain-boundary properties and to model materials response. The distributions of interfaces in multiphase materials have not been examined to the extent that single-phase materials have been investigated and role of grain-boundary complexions in determining microstructure have not been fully explored. Each of these issues will be described briefly below.

(1) Grain-Boundary Connectivity

While studies of boundary distributions have been successful in defining which types of grain boundaries are present in a polycrystal, much less is known about how the boundaries are connected. There have been several attempts to classify the connectivity of grain boundaries based upon triple junction types, twin clusters, and percolation metrics.[89–98] The mathematical tools of topology have occasionally been used to quantify connectivity, but their applications has been limited.[99–104] However, a recent paper by Wanner *et al.*[105] takes a new approach and explores the topology of the mechanical response fields in simulated polycrystals. As part of this study, the authors used homology metrics to characterize the connectivity of grain boundaries in a simulated polycrystal with uniaxial symmetry. The requirement for such an analysis, not used in any of the previous studies, is knowledge of crystal orientations.

In two dimensions, there are two topological metrics that measure the number of independent pieces of the network (referred to as B_0) and the number of closed loops (referred to as B_1).[105] In the context of plane sections of grain boundary networks, B_0 measures groups of grain boundaries not connected to the rest of the network and B_1 measures continuous, closed paths of grain boundaries or the number of grains. It has recently been proposed that the ratio of B_0 to B_1, or the inverse connectivity, is a suitable metric for network connectivity.[106] The ratio varies with the subset of boundaries considered and its variation as a function of the disorientation angle threshold is a characteristic of the type of microstructure, providing information beyond that available from relative area measurements. As an example, Fig. 11 compares two Ni microstructures (reference and grain-boundary engineered) after separating the $\Sigma 3^n$ and non-$\Sigma 3^n$ boundaries. The network of $\Sigma 3^n$ boundaries in the reference sample is clearly disconnected and this is reflected in an inverse connectivity that is >1. On the other hand, the network of non-$\Sigma 3^n$ boundaries (Fig. 5(b)) is relatively connected and this is reflected in an inverse connectivity that is <1 and smaller than the value for the $\Sigma 3^n$ network. The situation is reversed for the grain-boundary-engineered sample. In this case, the inverse connectivity is <1 for the $\Sigma 3^n$ boundaries. The inverse connectivity of the network of non-$\Sigma 3^n$ boundaries is 16 times larger, indicating that it is relatively disconnected compared with the network of $\Sigma 3^n$ boundaries. This suggests that the main impact of grain-boundary engineering is to increase the connectivity of twin related boundaries while simultaneously decreasing the connectivity of random boundaries. To establish connections to materials properties, it is necessary to carry out this analysis in three dimensions.

(2) Orientation Mapping by X-Rays

The three-dimensional orientation maps described in Section II were obtained by combining serial sections of planar EBSD orientation maps to reconstruct a three-dimensional volume of

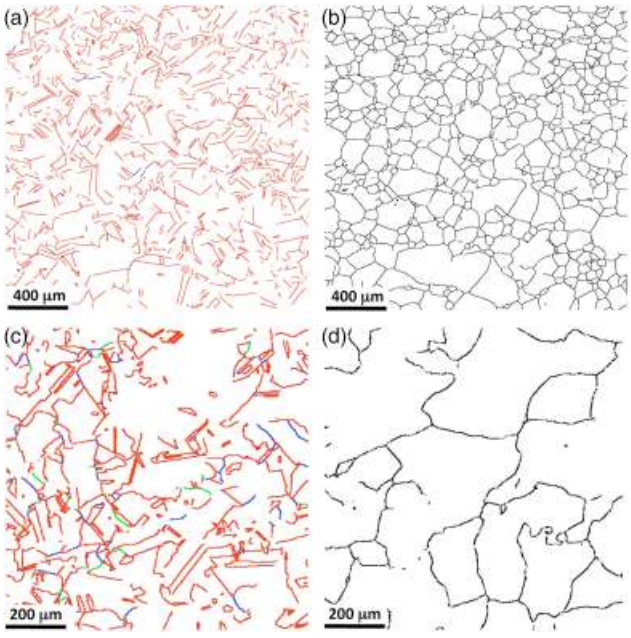

Fig. 11. Grain-boundary maps for the Ni samples. (a) All of the $\Sigma 3^n$ boundaries in the low $\Sigma 3$ Ni, $\beta_{01} = 3.1$, (b) all of the non-$\Sigma 3^n$ boundaries in the low $\Sigma 3$ Ni, $\beta_{01} = 0.12$, (c) all of the $\Sigma 3^n$ boundaries in high $\Sigma 3$ Ni, $\beta_{01} = 0.53$, (d) All of the non-$\Sigma 3^n$ boundaries in high $\Sigma 3$ Ni, $\beta_{01} = 8.6$. In (a) and (c) the $\Sigma 3$ boundaries are colored red, the $\Sigma 9$ boundaries are blue and the $\Sigma 27$ boundaries are green.[106]

material. This, as with manual serial sectioning, is a destructive technique and does not permit time dependent studies polycrystalline structure. There are, however, a number of emerging high-energy X-ray techniques that allow orientation maps to be determined from transmitted X-ray beams.[107–110] This makes it possible to create a three-dimensional orientation map, subject the sample to external stimulus (mechanical, chemical, thermal, or electrical) and map the structure again. An example of an orientation map recorded by high-energy diffraction microscopy (HEDM) is shown in Fig. 12; multiple slices of this type can be used to reconstruct a three-dimensional volume.[110] Transmission X-ray techniques have been used to study the shapes of recrystallizing grains,[111] the paths followed by cracks that advance by stress corrosion cracking,[109] and the evolution of grain shapes during grain growth in aluminum (R. M. Suter, personal communication, 2010). Compared with EBSD techniques, X-ray techniques have the significant advantage of being nondestructive and the disadvantages of lower resolution and more limited availability (because of the need for a synchrotron X-ray source).

(3) Computational Techniques for the Study of Grain-Boundary Networks

The role of computations in studies of grain boundaries and microstructures is rapidly expanding and will play an essential role in the advancement of microstructural science. In fact, the emerging discipline of Integrated Computational Materials Engineering relies on models that are reasonably accurate and able to describe complex, three-dimensional structures.[112] Among the many encouraging examples, a recent comparison of grain-boundary energies determined from experimental observations and from atomistic calculations provided useful information on the reliability and limitations of both techniques.[51,113–115] First, for cases where there were a sufficient number of experimental observations, there is reasonable agreement between the experiments and the measurements, as illustrated in Fig. 13. This agreement provides confidence in both the experimental and computational methods. Because the reliability of the experimental data depends upon the number of observations, the calculations presumably provide more reliable values for boundaries that are infrequently observed in the real samples. Conversely, the experiment provides reliable values for some commonly observed boundaries that are challenging to simulate because of the size of the repeat unit.

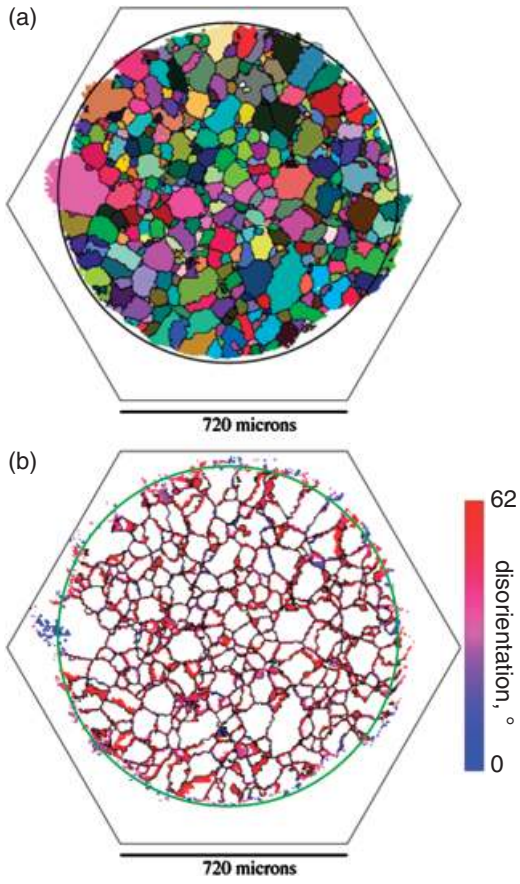

Fig. 12. (a) Orientation map of high purity Ni determined by HEDM. Orientations have been mapped to a color scale so that regions of similar color have similar crystallographic orientations. Black lines in the maps show mesh edges separating triangles with a more than 2° disorientation. The circles are guides to the eye showing the 1.1 mm diameter of the sample. (b) Element-to-element misorientation map comparing the layer shown in (a) and an adjacent one displaced by ten microns. Only misorientations $>0.5°$ are drawn, hence regions that are inside the same grain in both layers are white. Colors indicate boundaries inclined with respect to the sample plane and the scale indicates the amount of disorientation.[110]

Image-based simulations of polycrystals is an emerging method for probing the links between structure and a material's response.[54,55,116] The most attractive feature of this technique is that by using real microstructures as the basis for the calculations, the results are subject to validation. Once the calculations have been validated by experiment, it is then possible to explore the properties of hypothetical structures that have not yet been produced. In the past, calculations were generally limited to two-dimensional cases, mainly because the vast majority of images were also two-dimensional.[117–119] With three-dimensional data more readily available, simulations have also become three dimensional and this is essential to capture properties that depend upon the connectivity of microstructural features. Analysis of the relationship between stresses and microstructural features indicates that both high and low stress regions occur in close proximity to grain boundaries.[55]

(4) Interface Distributions in Multiphase Materials

While progress in understanding the GBCD for single-phase materials has been recounted above, very little is known about

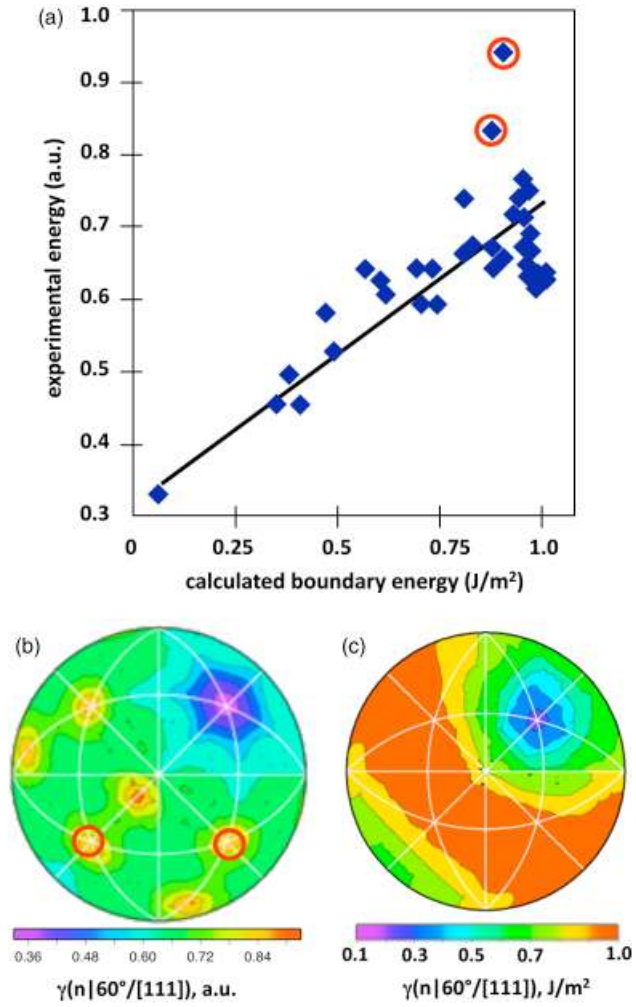

Fig. 13. (a) The relationship between the experimental and calculated grain-boundary energy for Σ3 grain boundaries in Ni. The two circled points are outliers. (b) The experimental energy distribution, the circled positions correspond to the circled points in (a). (c) Contour plot of calculated energies for comparison to (b). Because the maxima in the experimental energy distribution do not correspond to minima in the experimental population distribution, these points are considered questionable.[115]

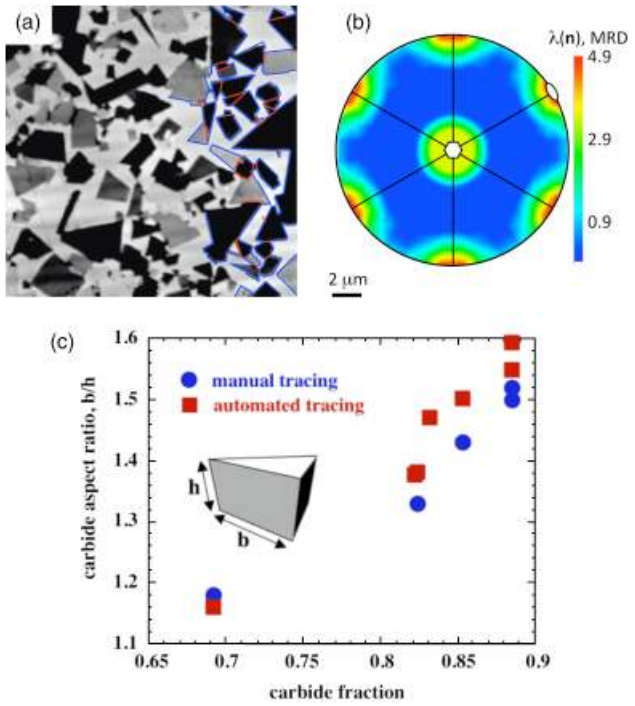

Fig. 14. (a) An atomic force microscope image of a WC/Co composite after etching. The dark polygonal features are WC grains. (b) IPD for the WC/Co interfaces in a WC/Co composite, showing that particles are dominantly bound by basal and prismatic surfaces. (c) Average base-to-height aspect ratios (b/h) for the carbide grains in the seven samples, plotted as a function of carbide volume fraction. Aspect ratios determined from manually traced line segments and automatically traced line segments show the trend that the average shape becomes more plate-like as the carbide volume fraction increases.[8]

the statistical distribution of interfaces in two-phase materials and composites. In a multiphase material, there is a GBCD for each crystalline phase, a phase boundary character distribution (PBCD) defining the relative areas of different types of boundaries between crystalline phases, and/or an interface plane distribution (IPD) for the case when a gaseous, liquid, or amorphous phase is present at the temperature where the composite is processed. The GBCD and PBCD have five independent crystallographic parameters and the IPD has two independent parameters. In all multiphased materials, there are at least two distinct distributions. While it is true that numerous solid–solid orientation relationships have been studied for specific cases, the statistical distribution of such interfaces in two-phase materials have been only very recently investigated.[8,25,120,121]

An example of a GBCD and IPD for the Co–WC system is shown in Fig. 14. Figure 14(a) shows an AFM image of polygonal WC crystals in Co, terminated by singular surfaces. In the right hand side of the image, the WC–Co boundaries have been artificially colored blue and the WC–WC grain boundaries artificially colored red. The IPD for the WC–Co boundaries is plotted in Fig. 14(b), indicating that interface planes are mostly (0001) and $(10\bar{1}0)$. This interface distribution changes with the Co volume fraction, as indicated by the change in the carbide aspect ratio in Fig. 14(c). Because there is no reason to suspect a change in the interfacial energies, there must be other factors that influence the distribution. In this case, the interface energies and the grain-boundary energies compete to achieve an ideal distribution and the final distribution of interfaces must result from a compromise; the principles governing this compromise are currently unclear.

(5) Complexions

The recent introduction of the concept of interface complexions, the subject of the most recent Sosman lecture by Harmer,[5] has transformed our view of the relationships between grain-boundary structure, composition, and properties.[5,122–130] As illustrated in Panel D, boundaries with different complexions can coexist in the same polycrystal and if one complexion has a much different grain-boundary mobility, a bimodal grain-size distribution results. Recent findings have illustrated that different complexions lead to distinct energy and grain-boundary plane distributions.[40,41]

One outstanding question has been, why is it that some boundaries enriched in solute undergo complexion transitions while others simply deposit the solute in the form of precipitate phases. A recent experiment has explored this issue and found that the relative energy of the interface between a precipitate and the host lattice affects the occurrence of complexion transitions.[39] Chemistries that produce low-energy interphase boundaries tend to suppress complexion transitions, while those nucleating precipitates with high interfacial energies promote them. This may be explained in the context of a phase selection competition in which the activation barrier to the complexion transition and precipitation compete with one another. The interphase boundary energies tend to be intermediate to the energies of the grain boundaries in the component systems. These facts lead to a proposed additive selection criterion based on

Panel D. Relationship between microstructure, grain boundary properties, and atomic structure of grain boundaries with different complexions.

The coexistence of multiple complexions can lead to a bimodal grain-size distribution if the mobilities of the complexions differ significantly. In this example of Nd-doped alumina, the boundaries in the SEM micrograph (a) are colored to differentiate high-mobility boundaries from low-mobility boundaries. Thermal groove measurements of the grain-boundary energies, colored in the same way (b), indicate that he high-mobility complexion has a lower energy.[40] The two complexions also have different grain-boundary orientation distributions (c, d).[41] HRTEM shows that the low-mobility boundary has a monolayer of segregated Nd and the high-mobility grain boundary has a bilayer of segregated Nd (e, f).[131] The two boundaries are said to have different complexions, because they are distinct in structure and composition.

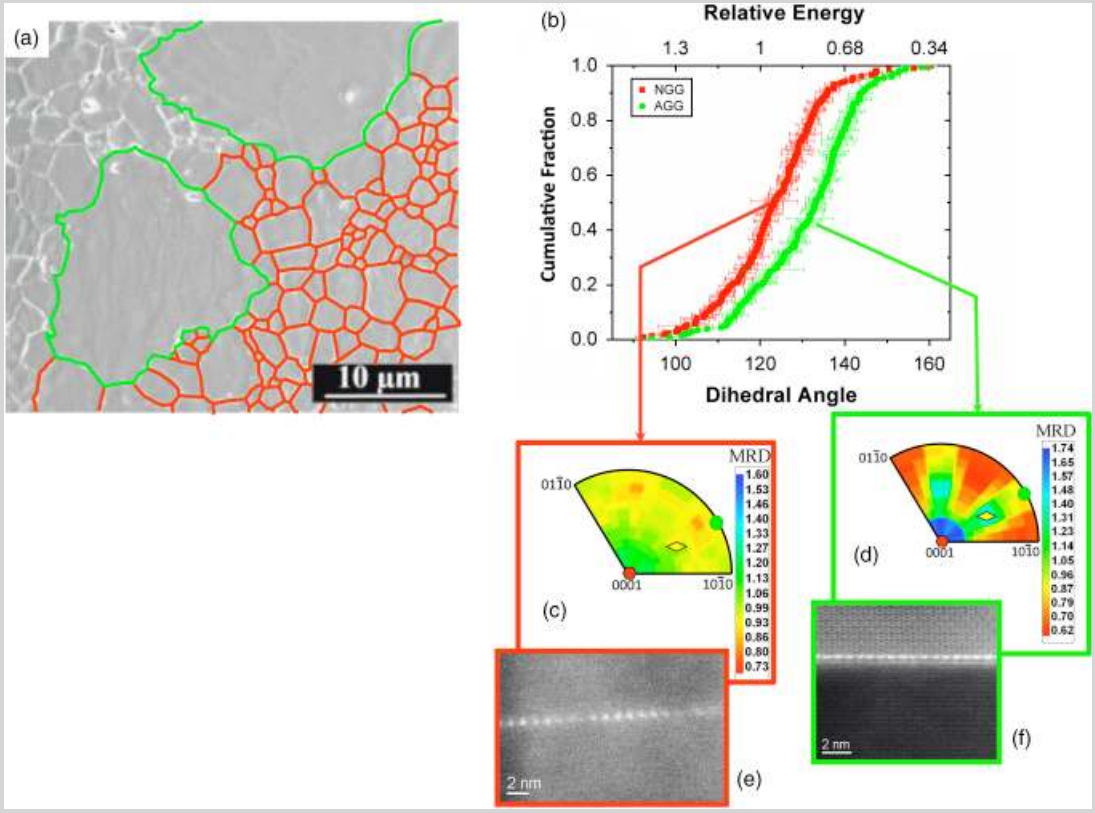

knowledge of interfacial energies. Namely, complexion transitions should be sought in systems where the solute strongly segregates to the boundary and where precipitates with coherent, low-energy interfaces do not form.

(6) Rarely Occurring Features in Microstructures

While it is now possible to specify the most commonly occurring constituents in distributions of microstructural features, much less is known about features far from the mean values. While knowledge of the features close to the mean is sufficient for determining average materials properties, such as elastic response or thermal conductivity, it is the rare features far from the mean that frequently trigger dramatic changes in the microstructure, often with life-limiting consequences for applications. For example, recent simulations have shown that the long-term capacity of a rechargeable Li-ion battery depends on the extremes of the grain-size distribution in the anode and cathode and that Li dendrite formation, which leads to unpredictable battery behavior, occurs on the smallest grains.[131] Similarly, when the size distribution of grains that initiate fatigue cracks in a Ti alloy are compared with the overall size distribution, it is found that the initiating grains are larger than the mean.[132] Understanding crack initiation is complex because the stresses in a polycrystal are heterogeneous and failure is nucleated at one of the points of high stress; the basis for the selection of the crack initiation point has not been established. The complexion transitions described above that result in a discontinuous change in the grain-boundary mobility are another example of a phenomenon dominated by rare features in the microstructure.

It has been difficult to study rarely occurring features because it has not been possible to characterize enough grains. In microstructure characterization, there is always a compromise between resolution and the number of grains that can be observed; this is summarized by the schematic in Fig. 15. Each field in the figure estimates the compromise between the number of grains that can be characterized, the resolution of the measurement, and the ability of the technique to be automated and scaled. Among the currently available methods, the most facile is EBSD-FIB mapping. However, the speed of the current implementation limits the field of view to the area surrounded by the blue line. If one also considers HEDM capabilities, the range of current possibilities is approximately shown by the black rectangle and number of grains relevant to many processes is out of reach. This problem could be overcome if a broad ion beam (BIB) milling system was used with EBSD, so that the entire surface was milled at the same time, instead of very small areas milled in a serial fashion.[133] Another development possible for the future is to couple robotic metallography (RoboMet)[134] with Laue diffraction. Finally, improved data collection and reconstruction protocols are envisioned for the HEDM that will increase output rates by more than a factor of 10 and

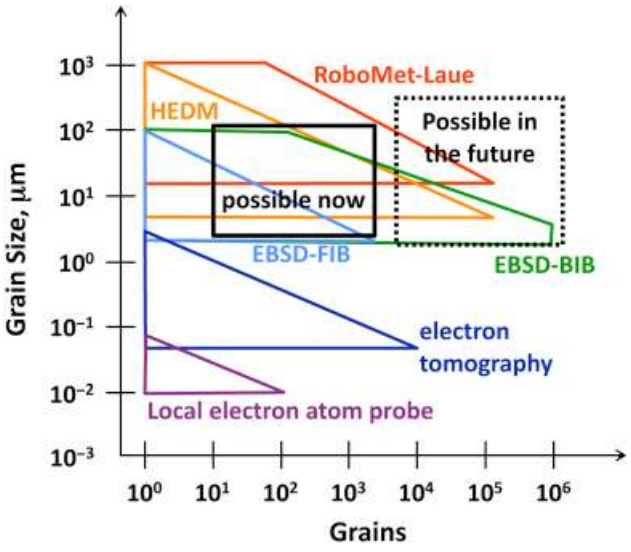

Fig. 15. Approximate limitations on the numbers of grains whose orientations can be mapped in three-dimensional using selected existing and proposed techniques. Those techniques with the greatest potential to record statistically significant numbers of grains are still in development.

correspondingly increase the volumes that can be mapped. While not currently possible, it is easy to imagine that progress in BIB-EBSD, HEDM, and RoboMet–Laue will make it possible to characterize 10^6 grains in the near future, as indicated by the box bounded by the dashed line.

VI. Summary

In the last decade, we have rapidly learned about how grain boundaries in materials are distributed in the five-dimensional space of grain-boundary types. The distribution is inversely correlated to the grain-boundary energy and the grain-boundary energy is determined more by the surface energies of the adjoining planes than by coincidence of the lattice. These findings provoke new questions at a time when both experimental and computational capabilities are rapidly expanding. During the next decade, it is likely that we will learn much more about how grain boundaries are connected, how grain boundary networks in single and multiphased materials form during processing, and how these networks influence macroscopic properties.

Acknowledgments

This work would not have been possible without the interdisciplinary collaborations fostered by the Materials Research Science and Engineering Center at Carnegie Mellon University. The findings I reviewed here resulted from interactions with mentors, colleagues, and students in the Center. While I cannot list them all, it is appropriate to cite the contributions of B. L. Adams, S. J. Dillon, M. P. Harmer, C. S. Kim, S. B. Lee, J. Li, H. M. Miller, W. W. Mullins, T. Sano, D. M. Saylor, A. D. Rollett, and P. Wynblatt.

References

[1]G. S. Rohrer, D. M. Saylor, B. El Dasher, B. L. Adams, A. D. Rollett, and P. Wynblatt, "The Distribution of Internal Interfaces in Polycrystals," *Z. Metallk.*, **95** [4] 197–214 (2004).
[2]G. S. Rohrer, "Influence of Interface Anisotropy on Grain Growth and Coarsening," *Ann. Rev. Mater. Res.*, **35**, 99–126 (2005).
[3]G. S. Rohrer, "The Distribution of Grain Boundary Planes in Polycrystals," *JOM*, **59** [9] 38–42 (2007).
[4]W. D. Kingery, "Plausible Concepts Necessary and Sufficient for Interpretation of Ceramic Grain-Boundary Phenomena-II, Solute Segregation, Grain-Boundary Diffusion, and General Discussion," *J. Am. Ceram. Soc.*, **57** [2] 74–83 (1974).
[5]M. P. Harmer, "Interfacial Kinetic Engineering: How Far have We Come Since Kingery's Inaugural Sosman Address," *J. Am. Ceram. Soc.*, **93** [2] 301–17 (2010).
[6]D. Brandon, "Defining Grain Boundaries: An Historical Perspective," *Mater. Sci. Technol.*, **26** [7] 762–73 (2010).
[7]C. Goux, "Structure des joints de grains: Considérations cristallographiques et méthodes de calcul des structures," *Can. Metall. Q*, **13** [1] 9–31 (1974).
[8]C. S. Kim, T. R. Massa, and G. S. Rohrer, "Interface Character Distributions in WC–Co Composites," *J. Am. Ceram. Soc.*, **91** [3] 996–1001 (2008).
[9]B. L. Adams, S. I. Wright, and K. Kunze, "Orientation Imaging—the Emergence of a New Microscopy," *Met. Trans. A*, **24** [4] 819–31 (1993).
[10]A. J. Schwartz, M. Kumar, B. L. Adams, and D. P. Field, *Electron Backscatter Diffraction in Materials Science*, 2nd edition, Springer, New York, 2009.
[11]K. Matsunaga, H. Nishimura, S. Hanyu, H. Muto, T. Yamamoto, and Y. Ikuhara, "HRTEM Study on Grain Boundary Atomic Structures Related to the Sliding Behavior in Alumina Bicrystals," *Appl. Surf. Sci.*, **241** [1–2] 75–9 (2005).
[12]S. Kimura, E. Yasuda, and M. Sakaki, "Grain Boundaries of MgO Bicrystals," *Yogyo-Kyokai-Shi*, **94** [8] 795–800 (1986).
[13]G. Dhalenne, M. Dechamps, and A. Revcolevschi, "Relative Energies of (011) Tilt Boundaries in NiO," *J. Am. Ceram. Soc.*, **65** [1] C11–2 (1982).
[14]C. S. Kim, A. D. Rollett, and G. S. Rohrer, "Grain Boundary Planes: New Dimensions in the Grain Boundary Character Distribution," *Scr. Mater.*, **54** [6] 1005–9 (2006).
[15]V. Randle and H. Davies, "A Comparison between Three-Dimensional and Two-Dimensional Grain Boundary Plane Analysis," *Ultramicroscopy*, **90** [2–3] 153–62 (2002).
[16]D. J. Rowenhorst and P. W. Voorhees, "Measurements of the Grain Boundary Energy and Anisotropy in Tin," *Metall. Mater. Trans. A—Phys. Metall. Mater. Sci.*, **36A** [8] 2127–35 (2005).
[17]D. M. Saylor, A. Morawiec, and G. S. Rohrer, "Distribution and Energies of Grain Boundaries in Magnesia as a Function of Five Degrees of Freedom," *J. Am. Ceram. Soc.*, **85** [12] 3081–3 (2002).
[18]D. M. Saylor, A. Morawiec, and G. S. Rohrer, "Distribution of Grain Boundaries in Magnesia as a Function of Five Macroscopic Parameters," *Acta Mater.*, **51** [13] 3663–74 (2003).
[19]D. M. Saylor, B. El Dasher, T. Sano, and G. S. Rohrer, "Distribution of Grain Boundaries in $SrTiO_3$ as a Function of Five Macroscopic Parameters," *J. Am. Ceram. Soc.*, **87** [4] 670–6 (2004).
[20]D. J. Rowenhorst, A. Gupta, C. R. Feng, and G. Spanos, "3D Crystallographic and Morphological Analysis of Coarse Martensite: Combining EBSD and Serial Sectioning," *Scr. Mater.*, **55** [1] 11–6 (2006).
[21]D. J. Rowenhorst, A. C. Lewis, and G. Spanos, "Three-Dimensional Analysis of Grain Topology and Interface Curvature in a Beta-Titanium Alloy," *Acta Mater.*, **58** [16] 5511–19 (2010).
[22]D. M. Saylor, B. S. El-Dasher, B. L. Adams, and G. S. Rohrer, "Measuring the Five-Parameter Grain-Boundary Distribution from Observations of Planar Sections," *Metall. Mater. Trans. A—Phys. Metall. Mater. Sci.*, **35A** [7] 1981–9 (2004).
[23]D. M. Saylor, B. El Dasher, Y. Pang, H. M. Miller, P. Wynblatt, A. D. Rollett, and G. S. Rohrer, "Habits of Grains in Dense Polycrystalline Solids," *J. Am. Ceram. Soc.*, **87** [4] 724–6 (2004).
[24]D. M. Saylor, B. S. El Dasher, A. D. Rollett, and G. S. Rohrer, "Distribution of Grain Boundaries in Aluminum as a Function of Five Macroscopic Parameters," *Acta Mater.*, **52** [12] 3649–55 (2004).
[25]E.P Gorzkowski, T. Sano, C. S. Kim, G. S. Rohrer, H. M. Chan, and M. P. Harmer, "Changes in the Distribution of Interfaces in PMN–35 mol % PT as a Function of Time," *Z. Metallk.*, **96** [2] 207–10 (2005).
[26]C. S. Kim, Y. Hu, G. S. Rohrer, and V. Randle, "Five-Parameter Grain Boundary Distribution in Grain Boundary Engineered Brass," *Scr. Mater.*, **52** [7] 633–7 (2005).
[27]V. Randle, Y. Hu, G. S. Rohrer, and C. S. Kim, "Distribution of Misorientations and Grain Boundary Planes in Grain Boundary Engineered Brass," *Mater. Sci. Technol.*, **21** [11] 1287–92 (2005).
[28]G. S. Rohrer, V. Randle, C. S. Kim, and Y. Hu, "Changes in the Five-Parameter Grain Boundary Character Distribution in Alpha-Brass Brought about by Iterative Thermomechanical Processing," *Acta Mater.*, **54** [17] 4489–502 (2006).
[29]V. Randle, "'Five-Parameter' Analysis of Grain Boundary Networks by Electron Backscatter Diffraction," *J. Microsc.*, **222**, 69–75 (2006).
[30]S. T. Downey, N. Bembridge, P. N. Kalu, H. M. Miller, G. S. Rohrer, and K. Han, "Grain Boundary Plane Distributions in Modified 316 LN Steel Exposed at Elevated and Cryogenic Temperatures," *J. Mater. Sci.*, **42**, 9543–7 (2007).
[31]V. Randle, G. S. Rohrer, and Y. Hu, "Five-Parameter Grain Boundary Analysis of a Titanium Alloy Before and After Low-Temperature Annealing," *Scr. Mater.*, **58** [3] 183–6 (2008).
[32]V. Randle, G. S. Rohrer, H. M. Miller, M. Coleman, and G. T. Owen, "Five-Para Meter Grain Boundary Distribution of Commercially Grain Boundary Engineered Nickel and Copper," *Acta Mater.*, **56** [10] 2363–73 (2008).
[33]R. Jones, V. Randle, and G. Owen, "Carbide Precipitation and Grain Boundary Plane Selection in Overaged Type 316 Austenitic Stainless Steel," *Mater. Sci. Eng. A—Struct. Mater. Prop. Microstruct. Process.*, **496** [1–2] 256–61 (2008).
[34]V. Randle, "Application of EBSD to the Analysis of Interface Planes: Evolution Over the Last Two Decades," *J. Microsc.*, **230** [3] 406–13 (2008).
[35]F. Papillon, G. S. Rohrer, and P. Wynblatt, "Effect of Segregating Impurities on the Grain-Boundary Character Distribution of Magnesium Oxide," *J. Am. Ceram. Soc.*, **92** [12] 3044–51 (2009).
[36]R. Jones, V. Randle, D. Engelberg, and T. J. Marrow, "Five-Parameter Grain Boundary Analysis of a Grain Boundary-Engineered Austenitic Stainless Steel," *J. Microsc.*, **233** [3] 417–22 (2009).
[37]G. M. Pennock, M. Coleman, M. R. Drury, and V. Randle, "Grain Boundary Plane Populations in Minerals: The Example of Wet NaCl after Low Strain Deformation," *Contrib. Mineral. Petrol.*, **158** [1] 53–67 (2009).
[38]V. Randle and R. Jones, "Grain Boundary Plane Distributions and Single-Step versus Multiple-Step Grain Boundary Engineering," *Mater. Sci. Eng. A—Struct. Mater. Prop. Microstruct. Process.*, **524** [1–2] 134–42 (2009).

[39]S. J. Dillon, M. P. Harmer, and G. S. Rohrer, "Influence of Interface Energies on Solute Partitioning Mechanisms in Doped Aluminas," *Acta Mater.*, **58** [15] 5097–108 (2010).
[40]S. J. Dillon, M. P. Harmer, and G. S. Rohrer, "The Relative Energies of Normally and Abnormally Growing Grain Boundaries in Alumina Displaying Different Complexions," *J. Am. Ceram. Soc.*, **93** [6] 1796–802 (2010).
[41]S. J. Dillon, H. Miller, M. P. Harmer, and G. S. Rohrer, "Grain Boundary plane Distributions in Aluminas Evolving by Normal and Abnormal Grain Growth and Displaying Different Complexions," *Inter. J. Mater. Res.*, **101** [1] 50–6 (2010).
[42]W. G. Wang, B. X. Zhou, G. S. Rohrer, H. Guo, and Z. X. Cai, "Textures and Grain Boundary Character Distributions in a Cold Rolled and Annealed Pb-Ca Based Alloy," *Mater. Sci Eng. A—Struct. Mater. Prop. Microstruct. Process.*, **527** [16–17] 3695–706 (2010).
[43]X. Y. Fang, W. G. Wang, G. S. Rohrer, and B. X. Zhou, "Grain Boundary Plane Distributions in the Cold-Rolled and Annealed Ferritic Stainless Steel," *Acta Metall. Sin.*, **46** [4] 404–10 (2010).
[44]W. W. ZX Cai, XY Fang, and H Guo, "Effect of Grain Size on the Grain Boundary Character Distributions of Cold Rolled and Annealed Pure Copper," *Acta Metall. Sin.*, **46** [7] 769–74 (2010).
[45]M. A. Groeber, B. K. Haley, M. D. Uchic, D. M. Dimiduk, and S. Ghosh, "3D Reconstruction and Characterization of Polycrystalline Microstructures using a FIB-SEM System," *Mater. Charact.*, **57** [4–5] 259–73 (2006).
[46]M. D. Uchic, M. A. Groeber, D. M. Dimiduk, and J. P. Simmons, "3D Microstructural Characterization of Nickel Superalloys Via Serial-Sectioning using a Dual Beam FIB-SEM," *Scr. Mater.*, **55** [1] 23–8 (2006).
[47]J. Konrad, S. Zaefferer, and D. Raabe, "Investigation of Orientation Gradients Around a Hard Laves Particle in a Warm-Rolled Fe_3Al-Based Alloy using a 3D EBSD-FIB Technique," *Acta Mater.*, **54** [5] 1369–80 (2006).
[48]M. Groeber, S. Ghosh, M. D. Uchic, and D. M. Dimiduk, "A Framework for Automated Analysis and Simulation of 3D Polycrystalline Micro Structures. Part 1: Statistical Characterization," *Acta Mater.*, **56** [6] 1257–73 (2008).
[49]M. Groeber, S. Ghosh, M. D. Uchic, and D. M. Dimiduk, "A Framework for Automated Analysis and Simulation of 3D Polycrystalline Micro Structures. Part 2: Synthetic Structure Generation," *Acta Mater.*, **56** [6] 1274–87 (2008).
[50]S. J. Dillon and G. S. Rohrer, "Characterization of the Grain-Boundary Character and Energy Distributions of Yttria using Automated Serial Sectioning and EBSD in the FIB," *J. Am. Ceram. Soc.*, **92** [7] 1580–5 (2009).
[51]J. Li, S. J. Dillon, and G. S. Rohrer, "Relative Grain Boundary Area and Energy Distributions in Nickel," *Acta Mater.*, **57** [14] 4304–11 (2009).
[52]G. S. Rohrer, J. Li, S. Lee, A. D. Rollett, M. Groeber, and M. D. Uchic, "Deriving Grain Boundary Character Distributions and Relative Grain Boundary Energies from Three-Dimensional EBSD Data," *Mater. Sci. Technol.*, **26** [6] 661–9 (2010).
[53]N. Zaafarani, D. Raabe, R. N. Singh, F. Roters, and S. Zaefferer, "Three-Dimensional Investigation of The Texture and Microstructure Below a Nanoindent in a Cu Single Crystal Using 3D EBSD and Crystal Plasticity Finite Element Simulations," *Acta Mater.*, **54** [7] 1863–76 (2006).
[54]A. C. Lewis, K. A. Jordan, and A. B. Geltmacher, "Determination of Critical Microstructural Features in an Austenitic Stainless Steel Using Image-Based Finite Element Modeling," *Metall. Mater. Trans. A—Phys. Metall. Mater. Sci.*, **39A** [5] 1109–17 (2008).
[55]A. D. Rollett, R. A. Lebensohn, M. Groeber, Y. Choi, J. Li, and G. S. Rohrer, "Stress Hot Spots in Viscoplastic Deformation of Polycrystals," *Modell. Simul. Mater. Sci. Eng.*, **18** [7] 074005, 16pp (2010).
[56]W. W. Mullins, "Theory of Thermal Grooving," *J. Appl. Phys.*, **28** [3] 333–9 (1957).
[57]C. Herring, "Surface Tension as a Motivation for Sintering"; pp. 143–79 in *The Physics of Powder Metallurgy*, Edited by W. E. Kingston. McGraw-Hill, New York, 1951.
[58]A. Morawiec, "Method to Calculate the Grain Boundary Energy Distribution over the space of Macroscopic Boundary Parameters from the Geometry of Triple Junctions," *Acta Mater.*, **48** [13] 3525–32 (2000).
[59]D. M. Saylor and G. S. Rohrer, "Measuring the Influence of Grain-Boundary Misorientation on Thermal Groove Geometry in Ceramic Polycrystals," *J. Am. Ceram. Soc.*, **82** [6] 1529–36 (1999).
[60]D. M. Saylor, D. Mason, and G. S. Rohrer, "Experimental Method for Determining Surface Energy Anisotropy and its Application to Magnesia," *J. Am. Ceram. Soc.*, **83** [5] 1226–32 (2000).
[61]D. M. Saylor, A. Morawiec, B. L. Adams, and G. S. Rohrer, "Misorientation Dependence of the Grain Boundary Energy in Magnesia," *Interface Sci.*, **8** [2–3] 131–40 (2000).
[62]D. M. Saylor and G. S. Rohrer, "Evaluating Anisotropic Surface Energies using the Capillarity Vector Reconstruction Method," *Interface Sci.*, **9** [1–2] 35–42 (2001).
[63]D. M. Saylor, A. Morawiec, and G. S. Rohrer, "The Relative free Energies of Grain Boundaries in Magnesia as a Function of Five Macroscopic Parameters," *Acta Mater.*, **51** [13] 3675–86 (2003).
[64]D. W. Hoffman and J. W. Cahn, "Vector Thermodynamics for Anisotropic Surfaces. 1. Fundamentals and Application to Plane Surface Junctions," *Surf. Sci.*, **31** [1] 368–88 (1972).
[65]J. W. Cahn and D. W. Hoffman, "Vector Thermodynamics for Anisotropic Surfaces. 2. Curved and Faceted Surfaces," *Acta Metall.*, **22** [10] 1205–14 (1974).
[66]H. M. Miller and G. S. Rohrer, "Evolution of the Grain Boundary Character Distribution in Strontium Titanate with Grain Growth"; pp. 343–54 in *Ceramic Transactions*, **Vol. 201**, Edited by A. D. Rollett. J. Wiley & Sons, Hoboken, 2009.
[67]M. L. Kronberg and F. H. Wilson, "Secondary Recrystallization in Copper," *Trans. AIMME*, **185** [8] 501–14 (1949).
[68]K. T. Aust and J. W. Rutter, "Grain Boundary Migration in High-Purity Lead and Dilute Lead-Tin Alloys," *Trans. AIMME*, **215** [1] 119–27 (1959).
[69]H. Grimmer, W. Bollmann, and D. H. Warrington, "Coincidence-Site Lattices and Complete Pattern-Shift Lattices in Cubic-Crystals," *Acta Crystallogr. Sect. A*, **A 30**, 197–207 (1974).
[70]G. S. Rohrer, B. S. El dasher, H. M. Miller, A. D. Rollett, and D. M. Saylor, "Distribution of Grain Boundary Planes at Coincident Site Lattice Misorientations"; pp. N7.2.1–11, in *MRS Spring Meeting. Vol. 819*, Edited by C. A. Schuh, M. Kumar, V. Randle, and C. B. Carter. Material Research Society Symposium Proceeding, Warrendale, PA, 2004.
[71]M. Kitayama and A. M. Glaeser, "The Wulff Shape of Alumina: III, Undoped Alumina," *J. Am. Ceram. Soc.*, **85** [3] 611–22 (2002).
[72]Y. Pang and P. Wynblatt, "Effects of Nb Doping and Segregation on the Grain Boundary Plane Distribution in TiO_2," *J. Am. Ceram. Soc.*, **89** [2] 666–71 (2006).
[73]T. Sano, D. M. Saylor, and G. S. Rohrer, "Surface Energy Anisotropy of $SrTiO_3$ at 1400 Degrees C in Air," *J. Am. Ceram. Soc.*, **86**, 1933–9 (2003).
[74]D. Wolf and S. Phillpot, "Role of the Densest Lattice Planes in the Stability of Crystalline Interfaces—A Computer-Simulation Study," *Mater. Sci. Engi. A—Struct. Mater. Prop. Microstruct. Process.*, **107**, 3–14 (1989).
[75]D. Wolf, "Correlation between Structure, Energy, and Ideal Cleavage Fracture for Symmetrical Grain-Boundaries in fcc Metals," *J. Mater. Res.*, **5** [8] 1708–30 (1990).
[76]A. P. Sutton, "An Analytic Model for Grain-Boundary Expansions and Cleavage Energies," *Philos. Mag. A—Phys. Condens. Matter Struct. Defects Mech. Prop.*, **63** [4] 793–818 (1991).
[77]A. P. Sutton, "Irrational Interfaces," *Prog. Mater. Sci.*, **36**, 167–202 (1992).
[78]W. T. Read and W. Shockley, "Dislocation Models of Crystal Grain Boundaries," *Phys. Rev.*, **78** [3] 275–89 (1950).
[79]M. M. Seabaugh, I. H. Kerscht, and G. L. Messing, "Texture Development by Templated Grain Growth in Liquid-Phase-Sintered Alpha-Alumina," *J. Am. Ceram. Soc.*, **80** [5] 1181–8 (1997).
[80]J. A. Horn, S. C. Zhang, U. Selvaraj, G. L. Messing, and S. Trolier-McKinstry, "Templated Grain Growth of Textured Bismuth Titanate," *J. Am. Ceram. Soc.*, **82** [4] 921–6 (1999).
[81]E. A. Holm, G. N. Hassold, and M. A. Miodownik, "On Misorientation Distribution Evolution During Anisotropic Grain Growth," *Acta Mater.*, **49** [15] 2981–91 (2001).
[82]A. Kazaryan, Y. Wang, S. A. Dregia, and B. R. Patton, "Grain Growth in Anisotropic Systems: Comparison of Effects of Energy and Mobility," *Acta Mater.*, **50** [10] 2491–502 (2002).
[83]M. Upmanyu, G. N. Hassold, A. Kazaryan, E. A. Holm, Y. Wang, B. Patton, and D. J. Srolovitz, "Boundary Mobility and Energy Anisotropy Effects on Microstructural Evolution During Grain Growth," *Interface Sci.*, **10** [2–3] 201–16 (2002).
[84]J. Gruber, D. C. George, A. P. Kuprat, G. S. Rohrer, and A. D. Rollett, "Effect of Anisotropic Grain Boundary Properties on Grain Boundary Plane Distributions During Grain Growth," *Scr. Mater.*, **53** [3] 351–5 (2005).
[85]S. J. Dillon and G. S. Rohrer, "Mechanism for the Development of Anisotropic Grain Boundary Character Distributions During Normal Grain Growth," *Acta Mater.*, **57** [1] 1–7 (2009).
[86]J. Gruber, G. S. Rohrer, and A. D. Rollett, "A model for the Origin of Anisotropic Grain Boundary Character Distributions in Polycrystalline Materials"; pp. 343–54 in *Applications of Texture Analysis. Vol. 201. Ceramic Transactions*, Edited by A. D. Rollett.. J. Wiley & Sons, Hoboken, NJ, 2009.
[87]J. Gruber, H. M. Miller, T. D. Hoffmann, G. S. Rohrer, and A. D. Rollett, "Misorientation Texture Development During Grain Growth. Part I: Simulation and Experiment," *Acta Mater.*, **57** [20] 6102–12 (2009).
[88]J. Gruber, A. D. Rollett, and G. S. Rohrer, "Misorientation Texture Development During Grain Growth. Part II: Theory," *Acta Mater.*, **58** [1] 14–9 (2010).
[89]M. Kumar, W. E. King, and A. J. Schwartz, "Modifications to the Microstructural Topology in F.C.C. Materials through Thermomechanical Processing," *Acta Mater.*, **48** [9] 2081–91 (2000).
[90]R. W. Minich, C. A. Schuh, and M. Kumar, "Role of Topological Constraints on the Statistical Properties of Grain Boundary Networks," *Phys. Rev. B*, **66** [5] 052101, 4pp (2002).
[91]M. Frary and C. A. Schuh, "Nonrandom Percolation Behavior of Grain Boundary Networks in High-T-c Superconductors," *Appl. Phys. Lett.*, **83** [18] 3755–7 (2003).
[92]C. A. Schuh, M. Kumar, and W. E. King, "Analysis of Grain Boundary Networks and their Evolution During Grain Boundary Engineering," *Acta Mater.*, **51** [3] 687–700 (2003).
[93]M. Frary and C. A. Schuh, "Percolation and Statistical Properties of Low- and High-Angle Interface Networks in Polycrystalline Ensembles," *Phys. Rev. B*, **69** [13] 134115, 12pp (2004).
[94]M. Frary and C. A. Schuh, "Connectivity and Percolation Behaviour of Grain Boundary Networks in Three Dimensions," *Philos. Mag.*, **85** [11] 1123–43 (2005).
[95]S. Xia, B. X. Zhou, W. J. Chen, and W. G. Wang, "Effects of Strain and Annealing Processes on the Distribution of Sigma 3 Boundaries in a Ni-Based Superalloy," *Scr. Mater.*, **54** [12] 2019–22 (2006).
[96]M. Frary, "Determination of Three-Dimensional Grain Boundary Connectivity from Two-Dimensional Microstructures," *Scr. Mater.*, **57** [3] 205–8 (2007).
[97]B. W. Reed, M. Kumar, R. W. Minich, and R. E. Rudd, "Fracture Roughness Scaling and Its Correlation with Grain Boundary Network Structure," *Acta Mater.*, **56** [13] 3278–89 (2008).
[98]S. A. Xia, B. X. Zhou, and W. J. Chen, "Effect of Single-Step Strain and Annealing on Grain Boundary Character Distribution and Intergranular Corrosion in Alloy 690," *J. Mater. Sci.*, **43** [9] 2990–3000 (2008).
[99]J. H. Steele, "Application of Topological Concepts in Sereology"; pp 39–58 in *Stereology and Quantitative Metallography*, Vol. 504, Edited by G. E. Pellissier and S. M. Purdy. ASTM stp American Society for Testing and Materials, Philadelphia, PA, 1972.

[100]K. R. Mecke, "Morphological Characterization of Patterns in Reaction–Diffusion Systems," *Phys. Rev. E*, **53** [5] 4794–800 (1996).
[101]K. R. Mecke and V. Sofonea, "Morphology of Spinodal Decomposition," *Phys. Rev. E*, **56** [4] R3761–64 (1997).
[102]R. Mendoza, I. Savin, K. Thornton, and P. W. Voorhees, "Topological Complexity and the Dynamics of Coarsening," *Nature Mater.*, **3** [6] 385–8 (2004).
[103]M. Gameiro, K. Mischaikow, and T. Wanner, "Evolution of Pattern Complexity in the Cahn–Hilliard Theory of Phase Separation," *Acta Mater.*, **53** [3] 693–704 (2005).
[104]R. Mendoza, K. Thornton, I. Savin, and P. W. Voorhees, "The Evolution of Interfacial Topology during Coarsening," *Acta Mater.*, **54** [3] 743–50 (2006).
[105]T. Wanner, E. R. Fuller, and D. M. Saylor, "Homology Metrics for Microstructure Response Fields in Polycrystals," *Acta Mater.*, **58** [1] 102–10 (2010).
[106]G. S. Rohrer and H. M. Miller, "Topological Characteristics of Plane Sections of Polycrystals," *Acta Mater.*, **58** [10] 3805–14 (2010).
[107]H. F. Poulsen, S. F. Nielsen, E. M. Lauridsen, S. Schmidt, R. M. Suter, U. Lienert, L. Margulies, T. Lorentzen, and D. J. Jensen, "Three-Dimensional Maps of Grain Boundaries and the Stress State of Individual Grains in Polycrystals and Powders," *J. Appl. Crystallogr.*, **34**, 751–6 (2001).
[108]B. C. Larson, W. Yang, G. E. Ice, J. D. Budai, and J. Z. Tischler, "Three-Dimensional X-ray Structural Microscopy with Submicrometre Resolution," *Nature*, **415** [6874] 887–90 (2002).
[109]A. King, G. Johnson, D. Engelberg, W. Ludwig, and J. Marrow, "Observations of Intergranular Stress Corrosion Cracking in a Grain-Mapped Polycrystal," *Science*, **321** [5887] 382–5 (2008).
[110]C. M. Hefferan, S. F. Li, J. Lind, U. Lienert, A. D. Rollett, P. Wynblatt, and R. M. Suter, "Statistics of High Purity Nickel Microstructure from High Energy X-Ray Diffraction Microscopy," *CMC—Comput. Mater. Continua*, **14** [3] 209–19 (2009).
[111]E. M. Lauridsen, D. J. Jensen, H. F. Poulsen, and U. Lienert, "Kinetics of Individual Grains During Recrystallization," *Scr. Mater.*, **43** [6] 561–6 (2000).
[112]J. E. Pollock, D. G. Bakman, M. C. Boyce, M. Gersh, E. A. Holm, R. LeSar, M. Long, A. C. Powel, J. J. Schirra, D. D. Whitis, and C. Woodward, *Integrated Computational Materials Engineering, A Transformational Discipline for Improved Competitiveness and National Security*. National Academies Press, Washington, DC, 2008.
[113]D. L. Olmsted, S. M. Foiles, and E. A. Holm, "Survey of Computed Grain Boundary Properties in Face-Centered Cubic Metals: I. Grain Boundary Energy," *Acta Mater.*, **57** [13] 3694–703 (2009).
[114]D. L. Olmsted, E. A. Holm, and S. M. Foiles, "Survey of Computed Grain Boundary Properties in Face-Centered Cubic Metals-II: Grain Boundary Mobility," *Acta Mater.*, **57** [13] 3704–13 (2009).
[115]G. S. Rohrer, E. A. Holm, A. D. Rollett, S. M. Foiles, J. Li, and D. L. Olmsted, "Comparing Calculated and Measured Grain Boundary Energies in Nickel," *Acta Mater.*, **58** [15] 5063–9 (2010).
[116]D. M. Saylor, E. R. Fuller, and T. Weiss, "Thermal-Elastic Response of Marble Polycrystals: Influence of Grain Orientation Configuration," *Int. J. Mater. Res.*, **98** [12] 1256–63 (2007).
[117]V. Vedula, S. Glass, D. Saylor, G. Rohrer, W. Carter, S. Langer, and E. Fuller, "Residual-Stress Predictions in Polycrystalline Alumina," *J. Am. Ceram. Soc.*, **84** [12] 2947–54 (2001).
[118]C. S. Kim, T. R. Massa, and G. S. Rohrer, "Modeling the Relationship between Microstructural Features and the Strength of WC-Co Composites," *Int. J. Refract. Met. Hard Mater.*, **24.**, 89–100 (2006).
[119]C. S. Kim, T. R. Massa, and G. S. Rohrer, "Modeling the Influence of Orientation Texture on the Strength of WC-Co Composites," *J. Am. Ceram. Soc.*, **90** [1] 199–204 (2007).
[120]T. Sano, C. S. Kim, and G. S. Rohrer, "Shape Evolution of $SrTiO_3$ Crystals During Coarsening in Titania-Rich Liquid," *J. Am. Ceram. Soc.*, **88** [4] 993–6 (2005).
[121]C. S. Kim and G. S. Rohrer, "Geometric and Crystallographic Characterization of wc Surfaces and Grain Boundaries in WC-Co Composites," *Interface Sci.*, **12** [1] 19–27 (2004).
[122]M. Tang, W. C. Carter, and R. M. Cannon, "Diffuse Interface Model for Structural Transitions of Grain Boundaries," *Phys. Rev. B*, **73** [2] 024102, 14pp (2006).
[123]M. Tang, W. C. Carter, and R. M. Cannon, "Grain Boundary Order–Disorder Transitions," *J. Mater. Sci.*, **41** [23] 7691–5 (2006).
[124]M. Tang, W. C. Carter, and R. M. Cannon, "Grain Boundary Transitions in Binary Alloys," *Phys. Rev. Lett.*, **97** [7] 075502, 4pp (2006).
[125]S. J. Dillon and M. P. Harmer, "Direct Observation of Multilayer Adsorption on Alumina Grain Boundaries," *J. Am. Ceram. Soc.*, **90** [3] 996–8 (2007).
[126]S. J. Dillon and M. P. Harmer, "Multiple Grain Boundary Transitions in Ceramics: A Case Study of Alumina," *Acta Mater.*, **55** [15] 5247–54 (2007).
[127]S. J. Dillon and M. P. Harmer, "Demystifying the Role of Sintering Additives with "Complexion"," *J. Eur. Ceram. Soc.*, **28** [7] 1485–93 (2008).
[128]S. J. Dillon and M. P. Harmer, "Relating Grain Boundary Complexion to Grain Boundary Kinetics ii: Silica-Doped Alumina," *J. Am. Ceram. Soc.*, **91** [7] 2314–20 (2008).
[129]S. J. Dillon and M. P. Harmer, "Relating Grain-Boundary Complexion to Grain-Boundary Kinetics I: Calcia-Doped Alumina," *J. Am. Ceram. Soc.*, **91** [7] 2304–13 (2008).
[130]S. J. Dillon, M. Tang, W. C. Carter, and M. P. Harmer, "Complexion: A New Concept for Kinetic Engineering in Materials Science," *Acta Mater.*, **55** [18] 6208–18 (2007).
[131]M. Smith, R. E. Garcia, and Q. C. Horn, "The Effect of Microstructure on the Galvanostatic Discharge of Graphite Anode Electrodes in LiCoO2-Based Rocking-Chair Rechargeable Batteries," *J. Electrochem. Soc.*, **156** [11] A896–904 (2009).
[132]S. K. Jha, J. M. Larsen, and A. H. Rosenberger, "Towards a Physics-Based Description of Fatigue Variability Behavior in Probabilistic Life-Prediction," *Eng. Fracture Mech.*, **76** [5] 681–94 (2009).
[133]G. Simons, K. Kunze, W. Hauffe, and J. Dual, "Three-Dimensional Microstructure of Thin Copper Foils Revealed by Ion Beam Cutting and Electron Backscatter Diffraction (EBSD)"; pp. 465–70 in *Texture and Anisotropy of Polycrystals II, Vol. 105. Solid State Phenomena*, Edited by C. Esling, M. Humbert, R.A Schwarzer, and F. Wagner. Transaction Publishers, New Brunswick, 2005.
[134]J. E. Spowart, H. M. Mullens, and B. T. Puchala, "Collecting and Analyzing Microstructures in Three Dimensions: A Fully Automated Approach," *JOM*, **55** [10] 35–7 (2003). □

Gregory S. Rohrer is the W. W. Mullins Professor of Materials Science and Engineering, the head of the Materials Science and Engineering Department, and the Director of the NSF sponsored Materials Research Science and Engineering Center at Carnegie Mellon University. He received his bachelor's degree in Physics from Franklin and Marshall College in 1984 and his Ph.D. in Materials Science and Engineering from the University of Pennsylvania in 1989. He has authored more than 170 publications and received the National Science Foundation Young Investigator Award (1994), the Roland B. Snow Award of the American Ceramic Society (1998), the Ross Coffin Purdy Award of the American Ceramic Society (2002), the Richard M. Fulrath Award of the American Ceramic Society (2004), and the Robert B. Sosman Award of the American Ceramic Society (2009). Rohrer gave the Lawley lecture at Drexel University in 2005, the Winchell Lecture at Purdue University in 2007, and was the G. E. Distinguished Lecture for MS&E, Rensselaer Polytechnic Institute in 2009. Rohrer is an Associate Editor of the Journal of the American Ceramic Society, chair of the Basic Science Division of the American Ceramic Society in 2005, and is currently chair of the University Materials Council.